LETTER

doi:10.1038/nature11541

Structural insight into the type-II mitochondrial NADH dehydrogenases

Yue Feng[1]*, Wenfei Li[1]*, Jian Li[1]*, Jiawei Wang[1], Jingpeng Ge[1], Duo Xu[1], Yanjing Liu[2], Kaiqi Wu[3], Qingyin Zeng[2], Jia-Wei Wu[1], Changlin Tian[3,4], Bing Zhou[1] & Maojun Yang[1]

The single-component type-II NADH dehydrogenases (NDH-2s) serve as alternatives to the multisubunit respiratory complex I (type-I NADH dehydrogenase (NDH-1), also called NADH:ubiquinone oxidoreductase; EC 1.6.5.3) in catalysing electron transfer from NADH to ubiquinone in the mitochondrial respiratory chain[1]. The yeast NDH-2 (Ndi1) oxidizes NADH on the matrix side and reduces ubiquinone to maintain mitochondrial NADH/NAD^+ homeostasis. Ndi1 is a potential therapeutic agent for human diseases caused by complex I defects[2–9], particularly Parkinson's disease, because its expression restores the mitochondrial activity in animals with complex I deficiency. NDH-2s in pathogenic microorganisms are viable targets for new antibiotics[10,11]. Here we solve the crystal structures of Ndi1 in its substrate-free, NADH-, ubiquinone- and NADH–ubiquinone-bound states, to help understand the catalytic mechanism of NDH-2s. We find that Ndi1 homodimerization through its carboxy-terminal domain is critical for its catalytic activity and membrane targeting. The structures reveal two ubiquinone-binding sites (UQ_I and UQ_{II}) in Ndi1. NADH and UQ_I can bind to Ndi1 simultaneously to form a substrate–protein complex. We propose that UQ_I interacts with FAD to act as an intermediate for electron transfer, and that NADH transfers electrons through this FAD–UQ_I complex to UQ_{II}. Together our data reveal the regulatory and catalytic mechanisms of Ndi1 and may facilitate the development or targeting of NDH-2s for potential therapeutic applications.

Electron transport chains, which comprise oxidative phosphorylation complexes I to V in the inner membrane of mitochondria, serve as the core components during respiration[12]. Complex I catalyses the transfer of two electrons from NADH to reduce ubiquinone to ubiquinol, and is the entry point for a large fraction of the electrons that traverse the respiratory chain[13,14]. This catalysis is the rate-limiting step in respiration and is central to energy metabolism[15]. Three different types of NDH are known: proton-pumping NDH (NDH-1); non-proton-pumping NDH (NDH-2); and the rare sodium-pumping NDH, called NQR[1,15,16].

First identified in domestic yeast[17,18], NDH-2 is a ~50-kDa, monotopic membrane protein with no energy-transducing capacity. Subsequently, multiple NDH-2s were found in various fungi, plants and primitive eukaryotic cells[1,19]. Genome-wide analysis has shown that a majority of organisms, such as *Escherichia coli*, contain both NDH-1 and NDH-2. However, some species have only NDH-2 (Supplementary Fig. 1, Supplementary Data 1 and Supplementary Table 1). Ndi1, one of the NDH-2s in *Saccharomyces cerevisiae*, faces the inside surface of the mitochondrial inner membrane, similar to NDH-1[20]. Here we report the crystal structures of Ndi1 in its apo and substrate-bound states.

Ndi1 forms a globular α/β structure that can be divided into three domains (Fig. 1a and Supplementary Fig. 2). Similar to other NADH- and FAD-associated enzymes, Ndi1 contains two canonical Rossmann domains with an FAD molecule buried deep in the first one (residues 49–412, referred to as the active domain hereafter) (Fig. 1 and Supplementary Fig. 3). A search of the Dali database[21] revealed that the NADH- and FAD-associated enzymes are the closest structural homologues of the Ndi1 active domain, with most of them having a root mean squared deviation (r.m.s.d.) of less than 2 Å when compared with the Ndi1 active domain. The structures of Ndi1 and other NADH- and FAD-associated enzymes differ in their C-terminal domains (CTDs; Fig. 1b). Ndi1 CTD is highly conserved among NDH-2s from different species (Supplementary Fig. 2 and Supplementary Data 1 and 2) and contains three β-strands (β19–β21) and two α-helices (α15 and α16) (Fig. 1a and Supplementary Fig. 2). The two α-helices form a helix–turn–helix motif that extensively interacts with the active domain, whereas the three β-strands make fewer contacts with the active domain (Supplementary Fig. 4).

In all the structures, each asymmetric unit contains an Ndi1 homodimer (Fig. 2a). Interactions between the two Ndi1 monomers are mainly mediated through helix α16 of the CTD (Fig. 2b and Supplementary Fig. 5a, b), burying a surface area of 5,982 $Å^2$. Consistent with this, we eluted wild-type Ndi1 from a gel filtration column with a native molecular mass of ~150 kD, corresponding to the calculated size of an Ndi1 dimer (Supplementary Fig. 6a). The linear relationship between Ndi1 concentration and its activity indicated that a single enzyme catalysed the electron transfer reaction (Supplementary Fig. 6b). To investigate whether Ndi1 was oligomeric *in vivo*, we co-expressed Ndi1–FLAG and Ndi1–Myc proteins in yeast cells and performed immunoprecipitation assays. As shown in Fig. 2c, the two Ndi1 proteins interacted with each other, indicating that Ndi1 formed an oligomer in yeast cells. Deletion of α16 compromised the interaction between Ndi1–FLAG and Ndi1–Myc, and deletion of both α15 and α16 abolished the interaction (Fig. 2c). This result indicated that the CTD is important for Ndi1 oligomerization. We further confirmed the functional importance of the CTD through a rescue assay. The plasmid carrying wild-type Ndi1 but not the mutants with α16 or α15 and α16 deleted, rescued the yeast *ndi1*Δ phenotype (Supplementary Fig. 5c). Thus, Ndi1 functions as a homodimer both *in vitro* and *in vivo*.

The membrane anchoring of *E. coli* NDH-2 is required for its activities[22]. One side of the Ndi1 homodimer contains a large hydrophobic surface, which is formed by the solvent-exposed residues from the CTD and surrounded by numerous positively charged patches (Fig. 2a, d). In solution, the hydrophobic surface was shielded by the detergent molecules used for protein purification, because several detergent molecules bound to this region in the structures of Ndi1 (Supplementary Fig. 7). This suggested that the hydrophobic surface could have a role in the mitochondrial membrane localization of Ndi1. Indeed, fractionation indicated that wild-type Ndi1 protein was exclusively found in the membrane fraction. In contrast, a large pool of the

[1]State Key Laboratory of Biomembrane and Membrane Biotechnology, Tsinghua-Peking Center for Life Sciences, School of Life Sciences, Tsinghua University, Beijing 100084, China. [2]State Key Laboratory of Systematic and Evolutionary Botany, Institute of Botany, Chinese Academy of Sciences, Beijing 100093, China. [3]Hefei National Laboratory for Physical Sciences at Microscale, School of Life Sciences, University of Science and Technology of China, Hefei, Anhui 230026, China. [4]High Magnetic Field Laboratory, Chinese Academy of Sciences, Hefei, Anhui 230031, China.
*These authors contributed equally to this work.

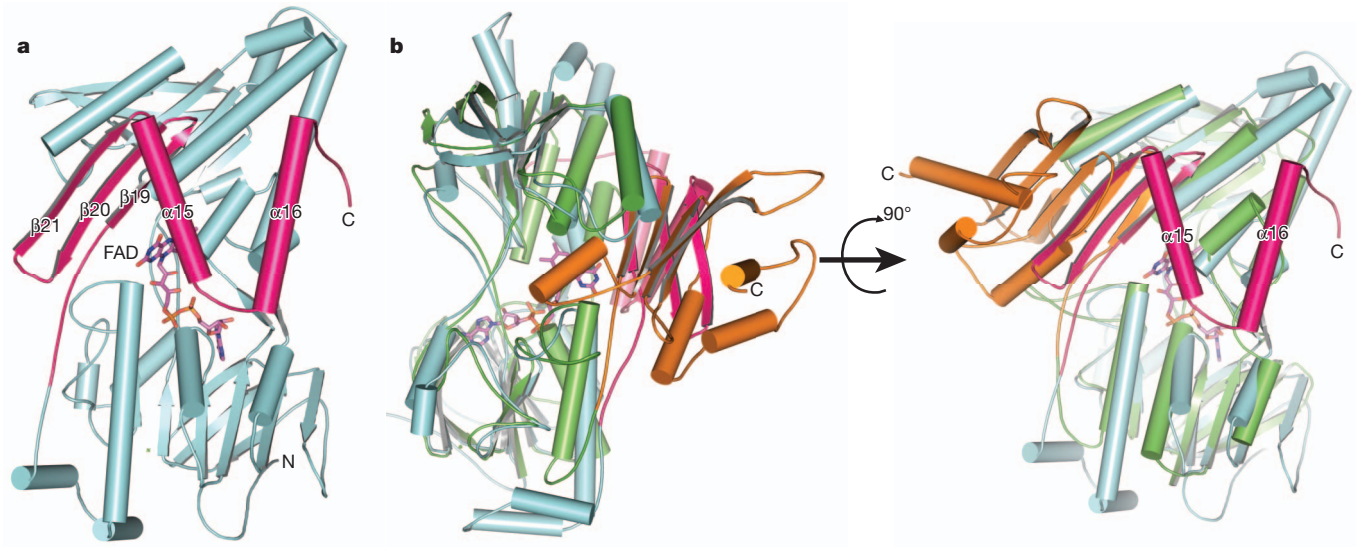

Figure 1 | Ndi1 has a unique CTD. **a**, Overall structure of Ndi1. The CTD (residues 439–513) of Ndi1 is coloured in pink and the active domain in cyan. FAD is shown in stick representation. **b**, Two views of the structural alignment between Ndi1 and the Pdr–Pdx complex from *Pseudomonas putida* (Protein Data Bank ID, 3LB8). The CTD of Pdr is coloured in orange and the remaining part in green. Colour codes for Ndi1 are the same as those in **a**.

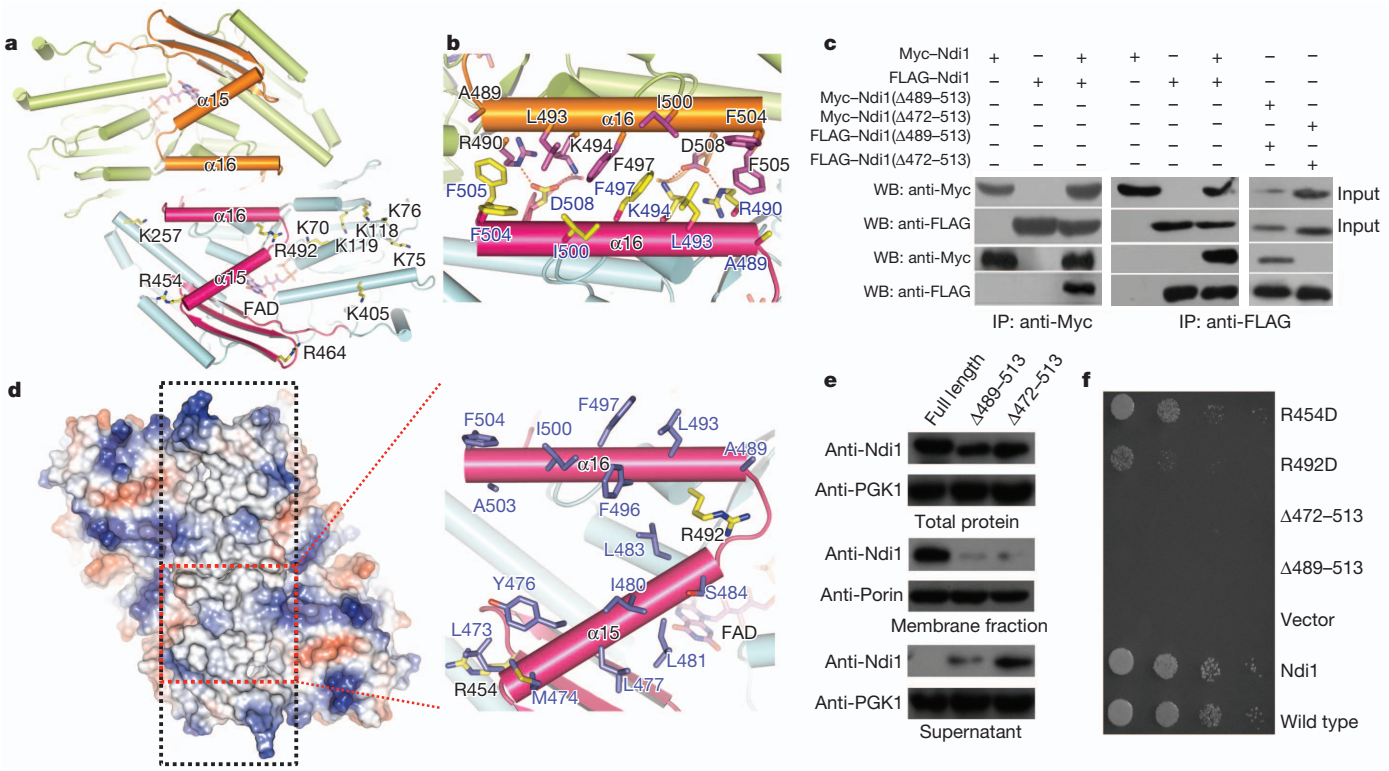

Figure 2 | The CTD mediates Ndi1 homodimerization and membrane attachment. **a**, Ndi1 forms a homodimer in crystals. One protomer is coloured as in Fig. 1a and the other one is coloured in orange (CTD) and lime (remainder). The conserved, positively charged residues on the membrane attachment side of one protomer are shown as yellow sticks. **b**, Detailed interactions between α16 of the two Ndi1 protomers. **c**, Ndi1 forms a dimer *in vivo*. Top: western blots of lysates (input) of *ndi1*Δ *trp1*Δ cells expressing the wild-type and the mutant forms of Ndi1–Myc, Ndi1–FLAG or both. Proteins were detected by western blot with anti-Myc and anti-FLAG antibodies. Bottom: Cell lysates in the top panels were subjected to anti-FLAG or anti-Myc immunoprecipitation (IP) followed by anti-Myc and anti-FLAG immunoblotting (WB). **d**, A large hydrophobic surface formed by the CTD in the Ndi1 homodimer. Left: electrostatic surface of the Ndi1 homodimer. The hydrophobic surface is highlighted with a dashed box. Right: the side chains of the surface residues from α15 and α16 of the CTD. For clarity, only one Ndi1 monomer is shown. **e**, The CTD is essential for Ndi1 membrane attachment. The lysates of *ndi1Δ* cells transformed with vectors encoding the indicated forms were fractionated into three samples: total protein, membrane fraction and supernatant. The samples were subjected to western blots. The loading amounts of the samples were examined using anti-Porin for the membrane fractions and anti-PGK1 antibody for the total protein and supernatant fractions. **f**, Mutations compromising Ndi1 membrane attachment cause growth defects in yeast cells.

mutant Ndi1 protein with α15 and α16 deleted was detected in the supernatant fraction (Fig. 2e), supporting a role for the two α-helices in Ndi1 membrane anchoring. The two α-helices were required for yeast viability, because their deletion resulted in a lethal phenotype (Fig. 2f).

We then solved the structure of the NADH-bound Ndi1. As observed in other NADH and FAD reductases, NADH binds to the second Rossmann domain and is fully accessible to FAD from the matrix side (Supplementary Fig. 8). Stabilized by a number of hydrogen-bonding interactions, NADH binding causes a slight conformational change in this domain (Supplementary Fig. 9a, b). Supporting their functional importance, single mutations of the NADH-interacting residues caused a lethal phenotype in yeast (Supplementary Fig. 9c). The nicotinamide ring of NADH is orientated in parallel with the *re*-face of the FAD isoalloxazine ring, with the distance between C4 of NADH and N5 of FAD being 3 Å, indicating that a direct electron transfer between them can occur.

The structure of the ubiquinone-bound form was determined by co-crystallizing Ndi1 with ubiquinone in the absence of NADH. One ubiquinone molecule (UQ_I) with a well-defined density is located close to FAD (Fig. 3a) and lies in the groove formed by β19–β21 and α15 from the CTD (Supplementary Figs 10a, b). The distance between the centre of the FAD isoalloxazine ring and UQ_I is about 7.8 Å. This site was occupied by a Triton X-100 (TRT) molecule in the apo structure (Supplementary Fig. 7), explaining why the protein extracted with *n*-dodecyl-β-D-maltopyranoside (DDM) but not with TRT contained bound ubiquinone[23,24]. Mutations of the residues that interact with UQ_I markedly attenuated the enzymatic activity of Ndi1 and compromised yeast survival (Supplementary Figs 10c, d). Although comparatively less well defined, a second ubiquinone molecule (UQ_{II}) was assigned to the stretch of density adjacent to UQ_I (Fig. 3a). This assignment was consistent with the recent studies indicating that Ndi1 contains both a bound ubiquinone and a catalytic ubiquinone at similar sites[24,25]. Both ubiquinone molecules are located on the *si*-face of the isoalloxazine ring of FAD and extend their aliphatic side chains towards the large hydrophobic surface (Supplementary Fig. 10a). The less well-defined UQ_{II} forms fewer contacts with Ndi1 than does UQ_I (Supplementary Fig. 10b).

Putidaredoxin reductase (Pdr) is an NADH-dependent enzyme and transfers electrons to P450 through forming a complex with the [2Fe–2S]-containing protein putidaredoxin[26] (Pdx). As anticipated, the structure of Pdr resembles that of the Ndi1 active domain. UQ_{II} in Ndi1 is similarly positioned relative to the [2Fe–2S] cluster in Pdx. The distance between the centre of the isoalloxazine ring and the UQ_{II} centre is about 11.2 Å, comparable to the 12 Å distance between FAD and the [2Fe–2S] cluster in the Pdr–Pdx complex (Supplementary Fig. 11). These structural observations suggest that it is spatially possible for the electron to be transferred from reduced FAD ($FADH_2$) to UQ_{II}.

Previous studies suggested that Ndi1 could form a ternary complex with NADH and ubiquinone[23]. We therefore soaked the ubiquinone-bound Ndi1 crystals with NADH and solved the structure of the Ndi1–NADH–ubiquinone complex (Fig. 3b). UQ_{II} was not observed in the complex. Because the crystals of the complex were obtained in the presence of oxygen, it might represent an enzyme–substrate complex

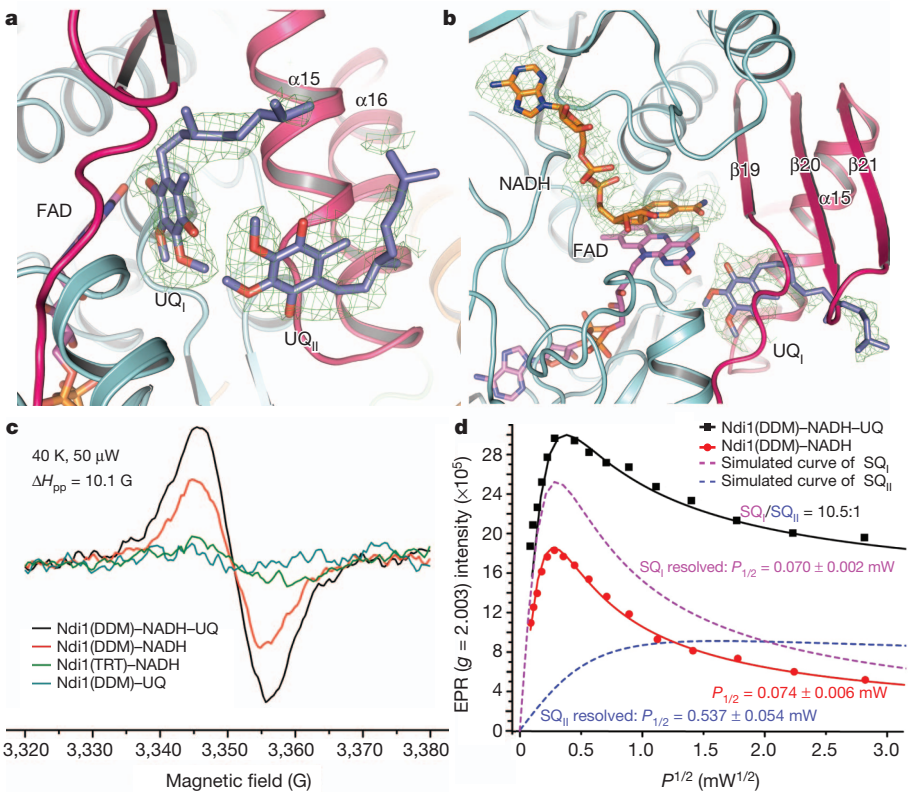

Figure 3 | Electron transfer of Ndi1 involves two ubiquinone molecules. **a**, Two ubiquinone molecules bind to Ndi1. The ubiquinone-binding sites in the Ndi1–ubiquinone complex are shown in ribbon representation. The ubiquinone and FAD molecules are shown as sticks and labelled. The $F_o - F_c$ omit density (green) is contoured at 3.5δ. **b**, Ribbon representation of the reaction centre in the Ndi1–NADH–ubiquinone complex. The $F_o - F_c$ omit density (green) is contoured at 3.5δ. **c**, Generation of Ndi1-catalysed radicals requires both NADH and ubiquinone. The EPR spectra of the $g = 2.003$ signals (g, electron g-factor) arise from ubisemiquinones of Ndi1 proteins as indicated. ΔH_{pp}, peak-to-peak width. **d**, Ndi1-catalysed generation of two populations of radicals. The power saturation behaviours of the $g = 2.003$ EPR signals of Ndi1 were monitored at 40 K. All experimental parameters except the microwave power were the same as in **c**. The ubisemiquinone signal of Ndi1(DDM)–NADH (red) was fitted by the equation described in Methods, and that of the sample with excessive ubiquinone (black) was resolved as the sum of two components. The theoretical curves for these two components are shown by the purple and blue dotted lines. Two sets of half-saturation parameters ($P_{1/2}$) and the relative concentration ratio are indicated.

rather than a metastable enzyme–intermediate complex. Comparison with the apo-Ndi1 structure shows that Ndi1 undergoes almost no conformational changes when bound by ubiquinones (r.m.s.d, 0.22 Å) or NADH–ubiquinone (r.m.s.d, 0.26 Å). The UQ_I-binding site is almost identical in the two structures, suggesting that UQ_I may act as a cofactor together with FAD to mediate electron transfer (Supplementary Fig. 12).

Our structures reveal that Ndi1 possesses a unique CTD (Fig. 1 and Supplementary Fig. 2) that mediates the Ndi1 dimerization required for its activity (Figs 2a–c and Supplementary Fig. 5). The CTD-mediated Ndi1 dimerization creates a large hydrophobic surface at one side (Fig. 2d) and a hydrophilic groove at the other (Supplementary Fig. 13). The biochemical assay (Figs 2e, f) supports there being a role for the hydrophobic surface in targeting Ndi1 to the mitochondrial membrane. The positively charged patches around the hydrophobic surface could also contribute to the membrane localization of Ndi1, presumably through interactions with the phosphate groups of membrane-localized phospholipids. Further investigations are needed to understand the specific mitochondrial membrane targeting of Ndi1. Additionally, the CTD is directly involved in the recognition of ubiquinones by Ndi1 (Figs 3a, b). Taken together, we conclude that the unique CTD of the single-component enzyme Ndi1 enables it to perform the electron transfer function of the multi-component NDH-1s.

Like many ubiquinone-reactive enzymes[27–30], Ndi1 has two ubiquinone-binding sites (Fig. 3a). UQ_I may not readily exchange with the ubiquinone pool, because it forms extensive interactions with the CTD of Ndi1. In contrast, UQ_{II} may better serve this purpose because it has much fewer contacts with Ndi1 (Supplementary Figs 10a, b). Our structures suggest that there is an electron transfer pathway from NADH to UQ_{II}, with UQ_I acting as an intermediate together with FAD. FAD first accepts two electrons from NADH to form $FADH_2$. Several possible mechanisms could be responsible for subsequent electron transfer. $FADH_2$ could transfer one electron to UQ_I and one to UQ_{II}, reducing both to ubisemiquinones. Then a disproportionation reaction between them could occur, restoring UQ_I to its previously oxidized state and converting UQ_{II} into ubiquinol. Alternatively, $FADH_2$ could transfer the electrons one by one to UQ_{II} through the bound UQ_I, reducing UQ_{II} to ubiquinol. It is also possible that $FADH_2$ transfers both electrons successively to UQ_I and that the two electrons are then further transferred to UQ_{II} consecutively. The net results of these three different pathways are the same: two electrons from NADH are transferred through the FAD–UQ_I complex to UQ_{II}. All three mechanisms involve ubisemiquinone radicals. Indeed, we detected the NADH–ubiquinone-dependent ubisemiquinone radicals in the Ndi1-catalysed electron transfer reaction using electron paramagnetic resonance (EPR) (Fig. 3c). Moreover, the power saturation experiments suggested the existence of two different populations of ubisemiquinone radicals (Fig. 3d). Future studies, such as EPR experiments at different pHs and redox titrations, are needed to establish the detailed electron transfer pathway of Ndi1.

Our study demonstrates that the electron transfer activity of the single-component Ndi1 is enabled by its unique CTD. Our data also support a model in which Ndi1 catalyses the electron transfer from NADH to UQ_{II} through a mechanism mediated by the FAD–UQ_I intermediate. This information could be valuable in guiding the engineering of Ndi1 for therapy and the design of antiparasitic inhibitors of NDH-2s.

METHODS SUMMARY

The wild-type and mutant forms of Ndi1 were expressed and purified from *E. coli* strain C43. Crystals were grown at 18 °C by the hanging-drop vapour diffusion method. Diffraction data sets were collected at beamline BL17U of the Shanghai Synchrotron Radiation Facility. The structures were solved by single-wavelength anomalous diffraction and molecular replacement methods. Data collection and structure refinement statistics are summarized in Supplementary Table 2. The EPR data were collected at the High Magnetic Field Laboratory of Chinese Academy of Sciences.

Full Methods and any associated references are available in the online version of the paper.

Received 29 April; accepted 29 August 2012.
Published online 21 October 2012.

1. Melo, A. M., Bandeiras, T. M. & Teixeira, M. New insights into type II NAD(P)H:quinone oxidoreductases. *Microbiol. Mol. Biol. Rev.* **68,** 603–616 (2004).
2. Sanz, A. *et al.* Expression of the yeast NADH dehydrogenase Ndi1 in *Drosophila* confers increased lifespan independently of dietary restriction. *Proc. Natl Acad. Sci. USA* **107,** 9105–9110 (2010).
3. Maas, M. F., Sellem, C. H., Krause, F., Dencher, N. A. & Sainsard-Chanet, A. Molecular gene therapy: overexpression of the alternative NADH dehydrogenase NDI1 restores overall physiology in a fungal model of respiratory complex I deficiency. *J. Mol. Biol.* **399,** 31–40 (2010).
4. Perales-Clemente, E. *et al.* Restoration of electron transport without proton pumping in mammalian mitochondria. *Proc. Natl Acad. Sci. USA* **105,** 18735–18739 (2008).
5. Marella, M., Seo, B. B., Flotte, T. R., Matsuno-Yagi, A. & Yagi, T. No immune responses by the expression of the yeast Ndi1 protein in rats. *PLoS ONE* **6,** e25910 (2011).
6. Marella, M., Seo, B. B., Yagi, T. & Matsuno-Yagi, A. Parkinson's disease and mitochondrial complex I: a perspective on the Ndi1 therapy. *J. Bioenerg. Biomembr.* **41,** 493–497 (2009).
7. Marella, M., Seo, B. B., Thomas, B. B., Matsuno-Yagi, A. & Yagi, T. Successful amelioration of mitochondrial optic neuropathy using the yeast NDI1 gene in a rat animal model. *PLoS ONE* **5,** e11472 (2010).
8. Barber-Singh, J., Seo, B. B., Matsuno-Yagi, A. & Yagi, T. Protective role of rAAV-NDI1, serotype 5, in an acute MPTP mouse Parkinson's model. *Parkinson's Dis.* **2011,** 438370 (2011).
9. Yagi, T. *et al.* Can a single subunit yeast NADH dehydrogenase (Ndi1) remedy diseases caused by respiratory complex I defects? *Rejuvenation Res.* **9,** 191–197 (2006).
10. Teh, J. S., Yano, T. & Rubin, H. Type II NADH: menaquinone oxidoreductase of Mycobacterium tuberculosis. *Infect. Disord. Drug Targets* **7,** 169–181 (2007).
11. Biagini, G. A. *et al.* Generation of quinolone antimalarials targeting the Plasmodium falciparum mitochondrial respiratory chain for the treatment and prophylaxis of malaria. *Proc. Natl Acad. Sci. USA* **109,** 8298–8303 (2012).
12. Rich, P. R. & Marechal, A. The mitochondrial respiratory chain. *Essays Biochem.* **47,** 1–23 (2010).
13. Efremov, R. G. & Sazanov, L. A. Structure of the membrane domain of respiratory complex I. *Nature* **476,** 414–420 (2011).
14. Walker, J. E. The NADH:ubiquinone oxidoreductase (complex I) of respiratory chains. *Q. Rev. Biophys.* **25,** 253–324 (1992).
15. Kerscher, S., Drose, S., Zickermann, V. & Brandt, U. The three families of respiratory NADH dehydrogenases. *Results Probl. Cell Differ.* **45,** 185–222 (2008).
16. Barquera, B., Zhou, W., Morgan, J. E. & Gennis, R. B. Riboflavin is a component of the Na+-pumping NADH-quinone oxidoreductase from Vibrio cholerae. *Proc. Natl Acad. Sci. USA* **99,** 10322–10324 (2002).
17. Ohnishi, T., Kawaguchi, K. & Hagihara, B. Preparation and some properties of yeast mitochondria. *J. Biol. Chem.* **241,** 1797–1806 (1966).
18. Ohnishi, T., Sottocasa, G. & Ernster, L. Current approaches to the mechanism of energy-coupling in the respiratory chain. Studies with yeast mitochondria. *Bull. Soc. Chim. Biol. (Paris)* **48,** 1189–1203 (1966).
19. Kerscher, S. J. Diversity and origin of alternative NADH:ubiquinone oxidoreductases. *Biochim. Biophys. Acta* **1459,** 274–283 (2000).
20. Seo, B. B. *et al.* Molecular remedy of complex I defects: rotenone-insensitive internal NADH-quinone oxidoreductase of *Saccharomyces cerevisiae* mitochondria restores the NADH oxidase activity of complex I-deficient mammalian cells. *Proc. Natl Acad. Sci. USA* **95,** 9167–9171 (1998).
21. Holm, L. & Rosenstrom, P. Dali server: conservation mapping in 3D. *Nucleic Acids Res.* **38,** W545–W549 (2010).
22. Villegas, J. M., Volentini, S. I., Rintoul, M. R. & Rapisarda, V. A. Amphipathic C-terminal region of *Escherichia coli* NADH dehydrogenase-2 mediates membrane localization. *Arch. Biochem. Biophys.* **505,** 155–159 (2011).
23. Yang, Y. *et al.* Reaction mechanism of single subunit NADH-ubiquinone oxidoreductase (Ndi1) from *Saccharomyces cerevisiae*: evidence for a ternary complex mechanism. *J. Biol. Chem.* **286,** 9287–9297 (2011).
24. Yamashita, T., Nakamaru-Ogiso, E., Miyoshi, H., Matsuno-Yagi, A. & Yagi, T. Roles of bound quinone in the single subunit NADH-quinone oxidoreductase (Ndi1) from *Saccharomyces cerevisiae. J. Biol. Chem.* **282,** 6012–6020 (2007).
25. Murai, M. *et al.* Characterization of the ubiquinone binding site in the alternative NADH-quinone oxidoreductase of *Saccharomyces cerevisiae* by photoaffinity labeling. *Biochemistry* **49,** 2973–2980 (2010).
26. Sevrioukova, I. F., Poulos, T. L. & Churbanova, I. Y. Crystal structure of the putidaredoxin reductase x putidaredoxin electron transfer complex. *J. Biol. Chem.* **285,** 13616–13620 (2010).
27. Ingledew, W. J., Ohnishi, T. & Salerno, J. C. Studies on a stabilisation of ubisemiquinone by *Escherichia coli* quinol oxidase, cytochrome *bo*. *Eur. J. Biochem.* **227,** 903–908 (1995).
28. Adelroth, P., Paddock, M. L., Sagle, L. B., Feher, G. & Okamura, M. Y. Identification of the proton pathway in bacterial reaction centers: both protons associated with

reduction of QB to QBH2 share a common entry point. *Proc. Natl Acad. Sci. USA* **97,** 13086–13091 (2000).
29. Okamura, M. Y., Paddock, M. L., Graige, M. S. & Feher, G. Proton and electron transfer in bacterial reaction centers. *Biochim. Biophys. Acta* **1458,** 148–163 (2000).
30. Ohnishi, T., Ohnishi, S. T., Shinzawa-Itoh, K., Yoshikawa, S. & Weber, R. T. EPR detection of two protein-associated ubiquinone components (SQ(Nf) and SQ(Ns)) in the membrane in situ and in proteoliposomes of isolated bovine heart complex I. *Biochim. Biophys. Acta* **1817,** 1803–1809 (2012).

Supplementary Information is available in the online version of the paper.

Acknowledgements We would like to thank the staff at beamline BL17U of the Shanghai Synchrotron Radiation Facility for their assistance with data collection. We thank W. Tong for maintenance and support of the EPR facility at the High Magnetic Field Laboratory, Chinese Academy of Sciences. This work was supported by the Ministry of Science and Technology of China (2011CB910502, 2011CB910900 and 2012CB911101), the National Natural Science Foundation of China (31030020 and 31170679) and Chinese Key Research Plan-Protein Sciences (2011CB911104).

Author Contributions M.Y. designed and directed the project. Y.F., W.L., J. W., J.G., D.X. and J.-W.W. purified the proteins, grew the crystals, collected data, solved the crystal structures and performed the *in vitro* activity analyses. Y.L. and Q.Z. performed the genome analysis of the NDHs. B.Z. and J.L. performed the *in vivo* biological analyses. Y.F., K.W. and C.T. performed the EPR analyses. M.Y. analysed the data and wrote the paper with the help of all the authors.

Author Information The atomic coordinates and structure factors of the apo-, NADH-, ubiquinone- and NADH–ubiquinone-bound forms of Ndi1 have been deposited in the Protein Data Bank under accession codes 4G6G, 4G6H, 4G74 and 4G73, respectively. Reprints and permissions information is available at www.nature.com/reprints. The authors declare no competing financial interests. Readers are welcome to comment on the online version of the paper. Correspondence and requests for materials should be addressed to M.Y. (maojunyang@tsinghua.edu.cn).

METHODS

Genome-wide analysis of phylogenetic relationships. NDH sequences from representative species of Prokaryota, Protista, Plantae, Fungi and Metazoa were used to investigate the evolutionary history of this gene family. Because some of the selected species were available only with draft genomes, two methods were used to obtain the sequences. The genes from completely sequenced genomes were obtained from KEGG (the Kyoto Encyclopedia of Genes and Genomes) ORTHOLOGY Database (KEGG ORTHOLOGY Entry K03885). (The locus tags of NDHs are listed in Supplementary Table 1.) The genes from draft genomes (*Saccharomyces mikatae* and *Saccharomyces bayanus*; see Supplementary Data 2) were identified by TBLASTN searches using three full-length NDH protein sequences of *S. cerevisiae*. The collected sequences were aligned using the MUSCLE (multiple sequence comparison by log-expectation) program[31]. The alignment was further adjusted manually using BIOEDIT[32]. Phylogenetic relationships among the NDHs were reconstructed using a maximum-likelihood procedure in PHYML[33] with the Jones–Taylor–Thornton amino-acid substitution model and 100 bootstrap replicates. (The tree and alignment are available as Supplementary Fig. 1 and Supplementary Data 1 and 2.) Furthermore, we obtained the subunit numbers of NADH:ubiquinone oxidoreductase (complex I) of each species from the KEGG PATHWAY Database (pathway entry, ko00190).

Protein expression and purification. The complementary DNA of Ndi1 from *S. cerevisiae* was cloned into pQE-80L vector. The Ndi1 mutants were generated by two-step PCR and were subcloned, overexpressed and purified in the same way as wild-type protein. Selenomethionine (Se-Met)-labelled protein was purified similarly. Overexpression of Ndi1 was induced in *E. coli* strain C43 using 0.5 mM isopropyl-β-D-thiogalactopyranoside when the cell density reached $D_{600\,nm}$ = 1.0. After growth for 10–12 h at 35 °C and 80 r.p.m., the cells were collected, homogenized in a buffer containing 50 mM Tris (pH 8.0) and 1 mM EDTA, and disrupted by sonication. Cell debris was removed by low-speed centrifugation for 15 min. The supernatant was collected and applied to ultracentrifugation at 150,000*g* for 1 h. The membrane fraction was collected and suspended in 50 mM Tris (pH 7.6), 200 mM NaCl, 0.1 mM EDTA and 10% glycerol (buffer A). After the addition of Triton X-100 at a final concentration of 0.3% (w/v) and 1 mM PMSF, the sample was incubated for 2 h with slow stirring at 4 °C. Following another ultracentrifugation step at 150,000*g* for 30 min, the supernatant was collected and loaded onto Ni^{2+}-nitrilotriacetate affinity resin (Ni-NTA, Qiagen) pre-equilibrated with buffer A containing 0.1% Triton X-100. Subsequently, the resin was washed three times, each time with 5 ml of buffer A containing 0.1% Triton X-100 and 8 mM histidine. Then the protein was eluted with buffer A containing 0.02% Triton X-100 and 200 mM histidine. The purified Ndi1 protein was concentrated and subjected to gel filtration chromatography (Superdex-200 10/30, GE Healthcare) in a buffer containing 25 mM Tris (pH 7.6), 300 mM NaCl, 5 mM DTT, 0.1 mM EDTA and 0.02% Triton X-100. The peak fractions were collected for biochemical analyses or crystallization.

Crystallization, data collection and structure determination. Crystals were grown at 18 °C by the hanging-drop method by mixing 1 μl of protein (10 mg ml^{-1}) with 1 μl of reservoir solution (3.8 M potassium formate, 2% w/v polyethylene glycol monomethyl ether 2,000 (pH 4.2 or 10.2)). The crystals appeared overnight and grew to full size in about four to five days. To obtain the NADH-bound Ndi1 crystals, we soaked the crystals in cryo-protectant with 10 mM NADH for about 1–3 min. To obtain the ubiquinone-bound Ndi1 crystals, we made fresh 50 mM ubiquinone-4 (UQ_4) stock solution in DMSO. Ndi1 and ubiquinone were co-crystallized with a final concentration of 0.5 mM UQ_4. To get the NADH–ubiquinone-bound Ndi1 crystals, we soaked the ubiquinone-bound Ndi1 crystals in cryo-protectant with 10 mM NADH for about 1–3 min. The crystals were then transferred to liquid nitrogen.

All the data were collected at Shanghai Synchrotron Radiation Facility beamline BL17U and were integrated and scaled using the HKL2000 package[34]. Further processing was carried out using programs from the CCP4 suite[35]. Data collection statistics are summarized in Supplementary Table 2. The self-rotation function with POLARRFN revealed a prominent peak at the section of $k = 180°$, indicating the presence of a non-crystallographic two-fold symmetry axis. SHELXD[36] was used to locate the positions of selenium sites, and HA_NCS[37] independently identified a two-fold non-crystallographic symmetry axis from the anomalous sites. The non-crystallographic symmetry from selenium sites has the same orientation as that from the self-rotation function, which verified the validity of the anomalous scatter positions. The identified anomalous scattering sites were input to PHASER[38] for single-wavelength anomalous diffraction phasing. The real-space constraints were applied to the electron density map in DM[39]. The final electron density map was of sufficient quality for BUCCANEER[40] to be able to build almost the complete model. The final model rebuilding was performed using COOT[41] and the protein structure was refined with PHENIX[42] against the high-resolution native data using non-crystallographic symmetry and stereochemistry information as restraints. Other structures were solved using molecular replacement. Data collection and structure refinement statistics are summarized in Supplementary Table 2.

Yeast strains and plasmids. The strains used in this study were derived from haploid strain BY4742 (*MATα his3*Δ1 *leu2*Δ0 *lys2*Δ0 *ura3*Δ0). *ndi1*Δ was generated by disruption of the *NDI1* gene through homologous recombination with KanMX4 as the replacement marker. Screen of positive colonies was achieved by spreading cells on YPD (yeast extract/peptone/dextrose) medium plus 0.4 mg ml^{-1} G418. Growth defects on YPG (yeast extract/peptone/glycerol) medium were used to confirm the disruption. *ndi1Δ trp1Δ* was generated by replacing the *TRP1* gene of *ndi1Δ* with *LEU2*. After selection on the SD-Leu medium, the colonies were further streaked on SD-Trp plates to confirm the deletion.

The vector pADH1–YES2 was modified from the pYES2 vector from Invitrogen, in which the *GAL1* promoter was replaced with an *ADH1* promoter for the purpose of constitutive expression of the target gene. pYES2–Ndi1 and pADH1–YES2–Ndi1 were generated by insertion of the complementary DNA of Ndi1 between the restriction sites EcoRI and XhoI of the vectors pYES2 and pADH1–YES2, respectively. The Ndi1 mutants were generated by two-step PCR and were subcloned into the two vectors using the same approach. To obtain pYES2–Myc–Ndi1 and pYES3–FLAG–Ndi1 constructs, DNA sequences corresponding to Myc (EQKLISEEDL) and FLAG (DYKDDDDK) tags were inserted into the complementary DNA sequence of Ndi1 of pYES2–Ndi1 and pYES3–Ndi1 constructs, respectively, just after its mitochondrial targeting sequence.

Yeast growth assay. For growth on agar plates, yeasts expressing wild-type and mutated *NDI1* genes in pYES2 or pADH1–YES2 vector were inoculated into liquid SD-Ura medium for overnight culture. After normalization of $D_{660\,nm}$ to 0.4, the cells were spotted in tenfold serial dilutions on SG-Ura and SD-Ura plates. The plates were incubated at 30 °C for three days before the pictures were taken. SD-Ura medium contains 2% (w/v) glucose, 0.5% (w/v) ammonium sulphate, 0.17% yeast nitrogen base with essential amino acids and other required nutrients except uracil. SG-Ura medium contains all the same components as SD-Ura except that the 2% (w/v) glucose is replaced with 2% (v/v) glycerol. For growth on agar plates, 2% agar was added.

Enzyme assays for Ndi1. The enzymatic activity of wild-type and mutant Ndi1 proteins was measured spectrophotometrically using NADH and UQ_1 as substrates. The standard assay was carried out at 30 °C in a 1.8-ml reaction mixture containing 50 mM MOPS (pH 7.0), 1 mM EDTA and varying amounts of NADH, UQ_1 and enzymes. Reactions were initiated by the addition of the enzyme to the reaction mixture. The progress of the reaction was monitored continuously by following the formation of NAD^+ at 340 nm, using a Lambda 45 spectrophotometer (PerkinElmer Life Sciences) equipped with a magnetic stirrer in the cuvette holder. The activities were determined using an extinction coefficient for NADH of 6,220 $cm^{-1}\,M^{-1}$ at 340 nm.

Co-immunoprecipitation experiments. Co-immunoprecipitation was performed as follows. For wild-type Ndi1, *ndi1Δ trp1Δ* cells were transformed with vectors pYES2–Myc–Ndi1 and pYES3–FLAG–Ndi1. After selection, the cells were grown in 50 ml of SGE-Ura medium to exponential phase before the cells were lysed by French press with extraction buffer (PBS, 0.1% Triton X-100 and protease inhibitor cocktail (Sigma)). The lysates were centrifuged at 15,000*g* for 30 min at 4 °C, and the supernatants were then incubated overnight with anti-FLAG or anti-Myc antibodies (Sigma) conjugated to protein A/G agarose. The agarose beads were washed three times with extraction buffer, boiled in SDS–polyacrylamide gel electrophoresis (PAGE) loading buffer, subjected to the SDS–PAGE and analysed by western blotting. Co-immunoprecipitation experiments for the truncated forms of Ndi1 were performed similarly.

Membrane fractionation. For membrane fractionation assay, *ndi1*Δ cells transformed with pYES2–Ndi1 vectors were cultured overnight in SD-Ura medium and then transferred to SGE-Ura. After growing to the exponential phase, cells were collected by centrifugation. The cells were broken in lysis buffer (PBS buffer with protease inhibitors), and after centrifugation at 4,300*g* for 15 min the supernatants were obtained as the sample of total proteins. The solution of total proteins was then further ultracentrifuged at 250,000*g* for 1 h, and the resulting supernatant and pellet taken as samples of supernatant and membrane fractions, respectively. The total protein, supernatant and membrane fractions were subjected to western blotting.

EPR characterization of ubisemiquinone radical. Four different samples prepared from Ndi1 proteins extracted using Triton X-100 (Ndi1-TRT) or DDM (Ndi1-DDM) were tested: NADH–UQ_1–Ndi1-DDM, NADH–Ndi1-DDM, NADH–Ndi1-TRT and UQ_1–Ndi1-DDM. All EPR samples were prepared in anaerobic conditions after purification of the Ndi1 protein. The Ndi1 protein was added to a final concentration of 50 μM and incubated with or without 5 mM UQ_1. After the addition of 2 mM NADH and incubation for 1 min, the sample was transferred to an EPR tube before a quick freezing to liquid-helium

temperature (around 2 K). EPR measurements were conducted on a Bruker X-band (9.4 GHz) EMSplus10/12 spectrometer. A cylindrical resonator (ER 4119hs TE011) was used for data collection. During EPR data acquisition, the sample temperature was maintained by an Oxford Instrument ESR 910 liquid-helium continuous-flow cryostat. A high-sensitivity EPR spectrum was obtained by temperature optimization from 2 to 200 K, and most of the EPR spectra were collected at an optimized temperature, 40 K. The EPR data acquisition parameters were as follows: modulation amplitude, 5.0 G; microwave power, 50 μW; sweep time, 40 s; time constant, 81.92 ms; sample temperature, 40 K.

A power saturation experiment was implemented with the microwave power ranging from 44 to 14 dB (or 8 μW to 8 mW) with a step size of 2 dB. The power saturation data was fitted following the equation $D=\sum_{i=1}^{n} C_i\sqrt{P}(1+P/P_{1/2,i})^{-0.5b_i}$, in which C_i is the relative concentration of the ith free radical, $P_{1/2,i}$ is the half-saturation parameter and b_i is the homogeneity parameter. All the EPR data were collected at the High Magnetic Field Laboratory of Chinese Academy of Sciences.

31. Edgar, R. C. MUSCLE: multiple sequence alignment with high accuracy and high throughput. *Nucleic Acids Res.* **32,** 1792–1797 (2004).
32. Hall, T. A. BioEdit: a user-friendly biological sequence alignment editor and analysis program for Windows 95/98/NT. *Nucleic Acids Symp. Ser.* **41,** 95–98 (1999).
33. Guindon, S. E. & Gascuel, O. A. Simple, fast, and accurate algorithm to estimate large phylogenies by maximum likelihood. *Syst. Biol.* **52,** 696–704 (2003).
34. Otwinowski, Z. & Minor, W. Processing of X-ray diffraction data collected in oscillation mode. *Methods Enzymol.* **276,** 307–326 (1997).
35. Collaborative Computational Project. Number 4. The CCP4 suite: programs for protein crystallography. *Acta Crystallogr. D* **50,** 760–763 (1994).
36. Schneider, T. R. & Sheldrick, G. M. Substructure solution with SHELXD. *Acta Crystallogr. D* **58,** 1772–1779 (2002).
37. Terwilliger, T. C. Rapid automatic NCS identification using heavy-atom substructures. *Acta Crystallogr. D* **58,** 2213–2215 (2002).
38. McCoy, A. J. *et al.* Phaser crystallographic software. *J. Appl. Crystallogr.* **40,** 658–674 (2007).
39. Cowtan, K. DM: an automated procedure for phase improvement by density modification. *CCP4 Newslett.* **31,** 34–38 (1994).
40. Cowtan, K. The Buccaneer software for automated model building. 1. Tracing protein chains. *Acta Crystallogr. D* **62,** 1002–1011 (2006).
41. Emsley, P. & Cowtan, K. Coot: model-building tools for molecular graphics. *Acta Crystallogr. D* **60,** 2126–2132 (2004).
42. Adams, P. D. *et al.* PHENIX: building new software for automated crystallographic structure determination. *Acta Crystallogr. D* **58,** 1948–1954 (2002).